Depletion of Cross-Stream Diffusion in the Presence of Viscoelasticity

Arman Sadeghi
Dept. of Mechanical Engineering, University of Kurdistan, Sanandaj 66177-15175, Iran

DOI 10.1002/aic.14955
Published online August 3, 2015 in Wiley Online Library (wileyonlinelibrary.com)

An effort to analyze the viscoelasticity effects on transverse transport of neutral solutes between two miscible streams in an electrokinetic T-sensor is presented. The analysis is based on an approximate analytical solution for the depthwise averaged concentration, assuming a channel of large width to depth ratio for which a one-dimensional profile is sufficient for describing the velocity field. We show that the solution derived is surprisingly accurate even for very small channel aspect ratios and the maximum error reduces to only about 1% when the aspect ratio is 5. The developed model reveals that the mixing length for a viscoelastic fluid may be by far larger than that for a Newtonian fluid. Moreover, the Taylor dispersion coefficient for electroosmotic flow of viscoelastic fluids, which its determination is a main part of the analysis, is found to be an increasing function of both the elasticity level and the EDL thickness.
 AIChE J, 61: 4533–4541, 2015
Keywords: electroosmotic flow, T-sensor, viscoelastic fluids, cross-stream diffusion

Introduction

Electrokinetics is a term used for referring to any type of motion that is the consequence of interaction between the ionic clouds, charged surfaces, and electric fields. Having been explored initially in the early 19th century,[1] the electrokinetic phenomena nowadays play an essential role in the development of many microfluidic devices such as modern micro total analysis systems called lab-on-a-chip (LOC) devices. LOCs are instruments that integrate several laboratory functions on a single chip of only millimeters to a few square centimeters in size.[2] On such a chip, the electrokinetic means based on electroosmosis, electrophoresis, and dielectrophoresis may be utilized so as to perform different functions such as transport, mixing, and separation. Electrokinetics offer many advantages over other flow actuation and species manipulation mechanisms including precise process control, low hydrodynamic dispersion, simple design and manufacturing of the pertinent devices, and the capability of easily integrating them into LOCs.

One of the essential tasks being performed in lab-on-a-chip instruments is the mixing of two or more fluids containing solutes of different concentrations with the aim of achieving a homogenous compound. Because of technological restrictions at microscale, simple micromixers such as the T-sensor are preferred over complex designs. A T-sensor, shown schematically in Figure 1, is a device with two inlets from which the streams to be mixed are supplied and a main channel within which these streams come into contact and run side by side. Mixing in a microfluidic T-sensor takes place primarily via molecular diffusion; nevertheless, the fluid velocity may strongly affect this cross-stream diffusion. This was first shown by Kamholz et al.[3–5] who reported a heterogeneous molecular diffusion due to the nonuniform velocity profile of a pressure driven flow. They demonstrated that the smallness of the residence time of the solutes traveling near centerline as compared to those located near the wall gives rise to butterfly shaped concentration contours.

The study of cross-stream diffusion in T/Y-shaped micromixers can be traced to the late 1990s. The relevant pioneering studies were conducted by Kamholz et al.[3–5] and Ismagilov et al.[6] A contemporary study by Beard[7] considered the Taylor dispersion of a solute in a microfluidic channel demonstrating that, despite axial molecular diffusion, axial dispersion due to the nonuniform velocity influences the distribution of solutes in the channel. Gobby et al.[8] showed that whereas throttling the fluid in a T-sensor considerably decreases the mixing length, altering the angle between the inlet channels does not significantly change the mixing performance. Shortly thereafter, Wang et al.[9] incorporated circular obstacles of different configurations into the main channel to improve the mixing efficiency. A microfluidic diffusion diluter was designed and characterized by Holden et al.[10] for the combinatorial study of concentration dependent phenomena. Subsequently, Wu et al.[11] and Lam et al.[12] presented simplified two-dimension (2-D) solutions for diffusive mixing in microchannels. More recently, Sullivan et al.[13] were able to closely predict the experimental data utilizing a lattice-Boltzmann-based numerical approach considering a concentration-dependent viscosity. One can also point out to more recent works dealing with molecular diffusion in a T/Y-sensor including both theoretical[14–21] and experimental[15–18] researches.

The previously mentioned research works were all dealing with pressure driven flow micromixers and the relevant works

Correspondence concerning this article should be addressed to A. Sadeghi at a.sadeghi@eng.uok.ac.ir.

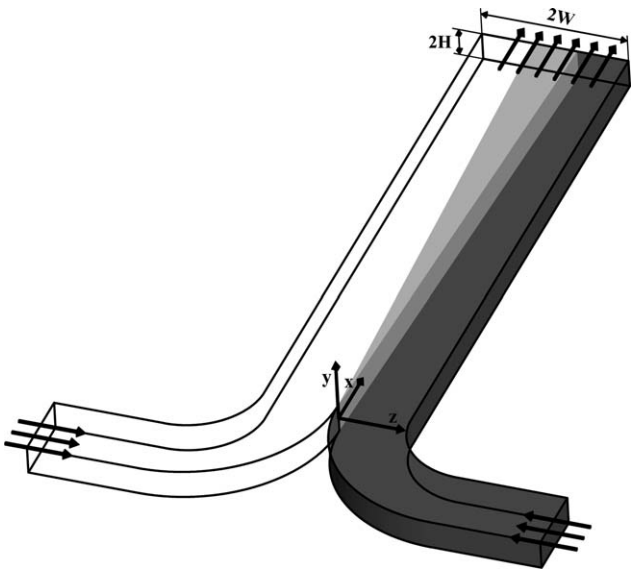

Figure 1. Schematic representation of the T-sensor including the dimensions along with the coordinate system.

are still scarce for electrokinetic-based devices. Erickson and Li[22] are among the firsts to perform a research in this scope. They conducted 3-D finite-element numerical simulations to analyze the influence of surface heterogeneity on mass transport in an electrokinetic T-sensor and discovered that the required mixing length can be reduced drastically utilizing surface heterogeneity. In a subsequent work, a model was proposed by Wang et al.[23] for the efficient and accurate simulations of laminar diffusion-based complex electrokinetic passive micromixers by representing them as a system of mixing elements of relatively simple geometry. More recently, Jeong et al.[24] developed a modified electrokinetic Y-shaped micromixer that involved the use of a periodic secondary voltage for mixing enhancement. In a recent numerical study, Ahmadian Yazdi et al.[25] paid attention to the influences of the shear-rate dependent rheology on the molecular diffusion in a Y-shaped micromixer utilizing a finite-difference numerical procedure.

The biofluids being tested in lab-on-a-chip devices contain different macromolecules which are the cause of their complicated rheological behavior. Accordingly, the Newton's law of viscosity is inadequate for describing the behavior of such complex fluids. Despite the considerable attention being given toward electrokinetic flow of non-Newtonian fluids and the associated mass transfer in the recent years,[26–32] the majority of the research works done on the subject matter of cross-stream diffusion have assumed a Newtonian rheology. The only exception is the work of Ahmadian Yazdi et al.[25] that considers the power-law viscosity model. The approach being undertaken in this work, however, is subject to inherent weaknesses of numerical analyses such as prohibitive computational costs, demanding large amount of data to deduce the governing law, and the difficulty of providing physical insights into the underlying transport mechanism. In addition, despite simple implementation and its effectiveness in a number of cases, the unphysical feature of an unbounded viscosity at zero shear rate is a main deficiency of the power-law model. The biofluid flows can more accurately be described utilizing the viscoelastic constitutive equations.[33] In this work, analytical solutions are derived for cross-stream mixing in a T-sensor utilizing the PTT and FENE-P viscoelastic rheological models. The analysis is based on the assumptions of small depthwise variations of the solute concentration and a 1-D velocity profile that both may be satisfied at large width to height ratios of the main channel. As a part of the analysis, the Taylor dispersion coefficient for electroosmotic flow of viscoelastic fluids is obtained for the first time and its functionality on the EDL thickness and the level of elasticity in the fluid is examined. The article is continued by studying the rheology effects on the mass transport characteristics and finally the conditions under which accurate data may be achieved from the solution are discussed by comparing the results with those predicted by full numerical simulations. The results of this investigation will give valuable insight into the transverse transport of different solutes such as protein and DNA molecules between coflowing streams of nonlinear biofluids that can be useful for design and active control of lab-on-a-chip devices.

Problem Formulation

We consider the viscoelasticity effects on the mixing characteristics in a T-sensor that is outlined in Figure 1. The flow is created by applying electroosmotic body force through an external electric field. The two inlet streams are of identical flow rates and include liquids with the same rheological properties, assumed to obey the PTT viscoelastic model. The liquid being injected from one of the inlets contains a solute with the concentration of c_0, whereas the other stream is free of solute. It is assumed that either the solute is electrically neutral or its electrophoretic transport is negligible as compared to the fluid electroosmotic velocity which is valid for species of very low electrophoretic mobility. We are interested in the concentration distribution of the solute downstream that is in the main channel wherein the flow is considered to be steady, laminar, and fully developed. This means that the entry length is neglected as compared to the mixing length because of the smallness of typical Reynolds numbers.[10] In addition, we suppose that the physical properties are all constant including the zeta potential which is also assumed to be uniformly distributed over the main channel walls and low enough to justify the use of the Debye–Hückel approximation. Finally, as it is usually the case in practical situations,[3,4] a high width to height ratio $\alpha=W/H$ is considered so that the flow in the main channel may be approximated by that between two flat plates distance $2H$ apart.

Electrical potential distribution

To predict the electroosmotic body force, an understanding of the variations of the EDL electrical potential, ψ, is crucial. Considering a solution containing $\mathbb{N}$ ionic species, the distribution of ψ, for our case, is governed by 1-D Poisson–Boltzmann equation, given as[34]

$$\frac{d^2\psi}{dy^2}=-\frac{\rho_e}{\varepsilon}=-\frac{e}{\varepsilon}\sum_{i=1}^{\mathbb{N}}\mathbb{z}_i n_{i0}\mathrm{e}^{\left(-\frac{e z_i \psi}{k_B T}\right)} \tag{1}$$

wherein ρ_e denotes the net charge density, ε is the permittivity constant of the solution, e stands for the proton charge and k_B, and T show the Boltzmann constant and the absolute temperature, respectively. In addition, $\mathbb{z}_i$ represents the valence number of the ith species of which the concentration at neutral conditions is given by n_{i0}. Equation 1 is nonlinear and cannot be solved analytically; nevertheless, for small potentials, it can

be linearized by expanding the exponential terms on the right-hand side in Taylor series and discarding all the terms that are quadratic or of higher order in ψ. This approximation, first introduced by Debye and Hückel,[35] has been shown to be valid for zeta potentials of up to 50 mV.[36] Making use of the electroneutrality conditions for $\psi=0$, the linearized form of the Poisson–Boltzmann equation becomes

$$\frac{d^2\psi}{dy^2}=\lambda_D^{-2}\psi \tag{2}$$

wherein $\lambda_D=\left(\sum_{i=1}^{\mathbb{N}} n_{i0}e^2\mathbb{z}_i^2/\varepsilon k_BT\right)^{-1/2}$ is the Debye length, a measure of the extent of EDL. The governing equation of the electrical potential can, therefore, be written in dimensionless form as

$$\frac{d^2\psi^*}{dy^{*2}}=\mathrm{K}^2\psi^* \tag{3}$$

where $\psi^*=\psi/\zeta$ with ζ being the zeta potential, $y^*=y/H$, and $\mathrm{K}=H/\lambda_D$ is the dimensionless Debye–Hückel parameter. The solution of Eq. 3 subject to the symmetry conditions at centerline and $\psi^*=1$ at the wall is given as

$$\psi^*=\frac{\cosh\left(\mathrm{K}y^*\right)}{\cosh\mathrm{K}} \tag{4}$$

Velocity distribution

The physical principle which governs the velocity distribution in a flowing fluid is the momentum conservation. Neglecting the pressure effects, the Cauchy momentum equation can be written as

$$\rho\frac{\mathrm{D}\mathbf{u}}{\mathrm{D}t}=\nabla\cdot\boldsymbol{\tau}+\mathbf{F} \tag{5}$$

in which ρ denotes the density, $\boldsymbol{\tau}$ represents the stress tensor, and $\mathbf{u}$ and $\mathbf{F}$ are the velocity and body force vectors, respectively. An understanding of the fluid rheological behavior is required so as to evaluate the stress components. The constitutive equation considered here is the simplified PTT model derived by Phan-Thien and Tanner[37,38] from network theory arguments which is given by

$$\Lambda(\tau_{kk})\boldsymbol{\tau}+\mathrm{Y}\boldsymbol{\tau}^{\nabla}=2\mu\dot{\boldsymbol{\gamma}} \tag{6}$$

where $\dot{\boldsymbol{\gamma}}=(\nabla\mathbf{u}^T+\nabla\mathbf{u})/2$ is the strain rate tensor, Y is the relaxation time of the fluid, μ is the viscosity coefficient, and $\boldsymbol{\tau}^{\nabla}$ represents the upper convected derivative of $\boldsymbol{\tau}$, defined as

$$\boldsymbol{\tau}^{\nabla}=\frac{\mathrm{D}\boldsymbol{\tau}}{\mathrm{D}t}-\nabla\mathbf{u}^T\cdot\boldsymbol{\tau}-\boldsymbol{\tau}\cdot\nabla\mathbf{u} \tag{7}$$

The stress coefficient function, $\Lambda(\tau_{kk})$, is given by the linear form[37]

$$\Lambda(\tau_{kk})=1+\epsilon\frac{\mathrm{Y}}{\mu}\tau_{kk} \tag{8}$$

where $\tau_{kk}=\tau_{xx}+\tau_{yy}+\tau_{zz}$ represents the trace of the stress tensor and ϵ is the extensibility coefficient. Since we consider a steady fully developed 1-D flow, the velocity vector reduces to $\mathbf{u}=[u_x(y),0,0]$ and the stress tensor becomes a function of y only; so $\mathrm{D}\mathbf{u}/\mathrm{D}t=\mathrm{D}\boldsymbol{\tau}/\mathrm{D}t=0$. It can be shown that, under these conditions, all the stress components vanish with the exceptions of τ_{xy} and τ_{yy} that are given as

$$\tau_{xy}=\frac{\mu}{\Lambda}\frac{du_x}{dy},\quad \tau_{yy}=\frac{2\mathrm{Y}\tau_{xy}}{\Lambda}\frac{du_x}{dy} \tag{9}$$

which on combination provide

$$\tau_{yy}=2\frac{\mathrm{Y}}{\mu}\tau_{xy}^2 \tag{10}$$

Leading to

$$\Lambda(\tau_{kk})=1+2\epsilon\frac{\mathrm{Y}^2}{\mu^2}\tau_{xy}^2 \tag{11}$$

In addition, from Eq. 9, the velocity gradient expression is derived as

$$\frac{du_x}{dy}=\frac{1}{\mu}\left(1+2\epsilon\frac{\mathrm{Y}^2}{\mu^2}\tau_{xy}^2\right)\tau_{xy} \tag{12}$$

with the following dimensionless form

$$\frac{du^*}{dy^*}=\tau^*+2\frac{\epsilon We^2}{\mathrm{K}^2}\tau^{*3} \tag{13}$$

Here, $u^*=u_x/u_{\mathrm{HS}}$, $\tau^*=H\tau_{xy}/\mu u_{\mathrm{HS}}$, and $We=\mathrm{Y}u_{\mathrm{HS}}/\lambda_D$ is the Weissenberg number, a measure of the level of elasticity in the fluid. The velocity scale used in these parameters is the Helmholtz–Smoluchowski electroosmotic velocity given as $u_{\mathrm{HS}}=-\varepsilon\zeta E_x/\mu$ wherein E_x is the electric field in the axial direction. It is now the time to turn our attention to the momentum equation. First, we evaluate the body force vector that is reduced to $\rho_e\mathbf{E}$, assuming a medium of constant permittivity. Utilizing $\rho_e=-\varepsilon\lambda_D^{-2}\psi=-\varepsilon d^2\psi/dy^2$, the momentum equation in the axial direction reduces to

$$\frac{d\tau_{xy}}{dy}=\varepsilon\lambda_D^{-2}E_x\psi \tag{14}$$

leading to the following dimensionless form

$$\frac{d\tau^*}{dy^*}=-\mathrm{K}^2\psi^*=-\mathrm{K}^2\frac{\cosh\left(\mathrm{K}y^*\right)}{\cosh\mathrm{K}} \tag{15}$$

Equation 15 may be solved subject to the zero shear stress condition at centerline to yield

$$\tau^*=-\mathrm{K}\frac{\sinh\left(\mathrm{K}y^*\right)}{\cosh\mathrm{K}} \tag{16}$$

Substituting Eq. 16 into Eq. 13 and solving the resultant equation subject to zero velocity condition at the wall, we come up with a dimensionless velocity in the form

$$u^*=a+b\cosh\left(\mathrm{K}y^*\right)+c\cosh^3\left(\mathrm{K}y^*\right) \tag{17}$$

where

$$a=1+\frac{2}{3}\epsilon We^2-2\frac{\epsilon We^2}{\cosh^2\mathrm{K}},\ b=2\frac{\epsilon We^2}{\cosh^3\mathrm{K}}-\frac{1}{\cosh\mathrm{K}},\ c=-\frac{2\epsilon We^2}{3\cosh^3\mathrm{K}} \tag{18}$$

The dimensionless mean velocity is also calculated as

$$u_m^*=\frac{u_m}{u_{\mathrm{HS}}}=\int_0^1 u^*\mathrm{d}y^*=a+\frac{b+c}{\mathrm{K}}\sinh\mathrm{K}+\frac{c}{3\mathrm{K}}\sinh^3\mathrm{K} \tag{19}$$

It is noteworthy that although the velocity profile given by Eq. 17 was obtained assuming a PTT model, it is also valid for FENE-P viscoelastic fluids provided generalized parameters are used.[33]

Concentration distribution

The general equation that governs solute transport in a nonreactive system is given as

$$\frac{\partial c}{\partial t}+\nabla\cdot(\mathbf{u}c)=\nabla\cdot(D\nabla c) \tag{20}$$

wherein c is the number concentration and D is the solute diffusivity. In general, an analytical treatment of Eq. 20 is very difficult to perform and, even for steady conditions, it is not possible to present a mathematically tractable analysis. Hence, additional simplifications have to be done to get an analytical solution. The problem physics dictates that the depthwise variations should be small. In addition, variations along the y-coordinate is of much less interest, as compared to the other two directions. Hence, at the expense of missing the depthwise variations in the concentration field, one can derive an approximate analytical solution for the present problem, utilizing an approach outlined by Taylor.[39] Neglecting axial molecular diffusion effects, Taylor demonstrated that a nonuniform velocity profile leads to a net axial diffusion of species. He proposed an effective diffusion coefficient for this phenomenon, latterly named Taylor dispersion coefficient in his honor.[40] Shortly thereafter, Aris proved that in general the effective diffusion coefficient is the sum of the molecular diffusion coefficient and the Taylor dispersion coefficient.[41]

Closely related to the present study, the essence of Taylor–Aris dispersion theory is that any approach based on an average concentration should account for the effective axial diffusivity arising from the neglect of the concentration variations along the direction throughout which the averaging is performed. As it was shown by Aris,[41] the Taylor dispersion coefficient depends on the flow and channel geometrical configuration; accordingly, the most important part of our modeling is to find out the effective diffusion coefficient for electroosmotic flow of viscoelastic fluids in a parallel plate microchannel. Along this line, following Taylor, we neglect axial molecular diffusion effects and begin with the modified mass transport equation for a fully developed flow in a moving reference frame, that is, $\tilde{x}=x-u_m t$, given as

$$\frac{\partial c}{\partial t}+(u-u_m)\frac{\partial c}{\partial \tilde{x}}=D\frac{\partial^2 c}{\partial y^2} \tag{21}$$

The time derivative here is taken at constant $\tilde{x}$ and, under the conditions required for the validity of the Taylor–Aris dispersion analysis, it may be neglected relative to the depthwise diffusion term.[42] Considering small depthwise variations, the term $\partial c/\partial\tilde{x}$ may be substituted by $dc_{da}/d\tilde{x}$ wherein $c_{da}(x)=\int_0^H c(x,y)dy/H$ is the depthwise averaged concentration.[42] Applying these assumptions, Eq. 21 reduces to

$$D\frac{\partial^2 c}{\partial y^2}=(u-u_m)\frac{\mathrm{d}c_{da}}{\mathrm{d}\tilde{x}} \tag{22}$$

which can be solved subject to zero mass flux conditions at $y=0$ to yield

$$c(x,y)=\frac{\mathrm{d}c_{da}/\mathrm{d}\tilde{x}}{D}\int_0^y\int_0^\xi[u(\eta)-u_m]\mathrm{d}\eta\mathrm{d}\xi+c(x,0) \tag{23}$$

where $c(x,0)$ is obtained by performing depthwise averaging of both sides of Eq. 23; thus, it is expressed as

$$c(x,0)=c_{da}(x)-\frac{\mathrm{d}c_{da}/\mathrm{d}\tilde{x}}{DH}\int_0^H\int_0^y\int_0^\xi[u(\eta)-u_m]\mathrm{d}\eta\mathrm{d}\xi\mathrm{d}y \tag{24}$$

Equation 23, expressing the variations of the solute concentration with y, was derived assuming a slit geometry; as such, it is not totally true to utilize it in in the present study because of the rectangular geometry of the mixing device. However, due to high width to depth ratio of the main channel, it holds everywhere except near the vertical walls. Neglecting the sidewall effects, we may use Eq. 23 in our modeling by considering c_{da} to be a function of x and z coordinates. Substituting this equation into the simplified form of Eq. 20 for steady and hydrodynamically developed conditions and performing the depthwise averaging, the following equation is reached

$$u_m\frac{\partial c_{da}}{\partial x}=D_{\mathrm{eff}}\frac{\partial^2 c_{da}}{\partial x^2}+D\frac{\partial^2 c_{da}}{\partial z^2} \tag{25}$$

where D_{eff} is the effective diffusivity given as

$$D_{\mathrm{eff}}=D\left\{1-Pe^2\int_0^1\left[u^*(y^*)-u_m^*\right]\int_0^{y^*}\int_0^\xi\left[u^*(\eta)-u_m^*\right]\mathrm{d}\eta\mathrm{d}\xi\mathrm{d}y^*\right\} \tag{26}$$

wherein $Pe=u_{\mathrm{HS}}H/D$ is the Peclet number. Equation 26 provides a formulation of the effective diffusivity for a parallel plate channel, irrespective of the velocity profile shape. Considering the velocity distribution (17), D_{eff} for electroosmotic flow of PTT/FENE-P viscoelastic fluids is expressed as

$$D_{\mathrm{eff}}=D\left\{1-Pe^2\left[\left(a-u_m^*\right)A_1+bA_2+cA_3\right]\right\} \tag{27}$$

with the following coefficients

$$\begin{aligned}A_1=&\frac{1}{54\mathrm{K}^3}[9(a-u_m^*)\mathrm{K}^3-(54b+42c)\mathrm{K}+(54b+40c)\mathrm{sinhK}\\&+2c\mathrm{sinhKcosh}^2\mathrm{K}]\end{aligned} \tag{28}$$

$$\begin{aligned}A_2=&\frac{1}{72\mathrm{K}^3}[36(a-u_m^*)(2\mathrm{sinhK}-2\mathrm{KcoshK}+\mathrm{K}^2\mathrm{sinhK})\\&+(36b+27c)(\mathrm{K}+\mathrm{sinhKcoshK})-(72b+56c)\mathrm{sinhK}\\&+2c\mathrm{sinhKcosh}^3\mathrm{K}]\end{aligned} \tag{29}$$

$$\begin{aligned}A_3=&\frac{1}{432\mathrm{K}^3}[8(a-u_m^*)(40\mathrm{sinhK}-42\mathrm{KcoshK}\\&+18\mathrm{K}^2\mathrm{sinhK}+2\mathrm{sinhKcosh}^2\mathrm{K}-6\mathrm{KcoshKsinh}^2\mathrm{K}\\&+9\mathrm{K}^2\mathrm{sinhKcosh}^2\mathrm{K})+(54b+41c)\\&(3\mathrm{K}+3\mathrm{sinhKcoshK}+2\mathrm{sinhKcosh}^3\mathrm{K})\\&-(144b+112c)(2\mathrm{sinhK}+\mathrm{sinhKcosh}^2\mathrm{K})\\&+8c\mathrm{sinhKcosh}^5\mathrm{K}]\end{aligned} \tag{30}$$

As noted by Aris,[41] D_{eff} for given species and geometric configurations is only a function of the factors that govern the velocity profile, which in our case include K and ϵWe^2. Equation 26 states that D_{eff} reduces to D for the so-called slug flow. This is because the concentration variations vanish in the presence of a uniform flow. This is confirmed by Eq. 27 which shows that $D_{\mathrm{eff}}\rightarrow D$ at high values of K for which EDL is so thin that the velocity profile is actually uniform, regardless of ϵWe^2. Similar to the electrical potential and velocity distributions, the species transport equation is made dimensionless utilizing the parameters $x^*=x/HPe$, $z^*=z/H$, $c^*=c_{da}/c_0$, and $D^*=D_{\mathrm{eff}}/D$ and the outcome is

$$u_m^*\frac{\partial c^*}{\partial x^*}=\frac{D^*}{Pe^2}\frac{\partial^2 c^*}{\partial x^{*2}}+\frac{\partial^2 c^*}{\partial z^{*2}} \tag{31}$$

The dimensionless concentration equation is constrained by the following boundary conditions

$$\left.\frac{\partial c^*}{\partial z^*}\right|_{z^*=\pm\alpha} = 0 \tag{32}$$

$$c^*|_{x^*=0} = \begin{cases} 0 & z^* < 0 \\ 1 & z^* \geq 0 \end{cases} \tag{33}$$

The general solution of Eq. 31 satisfying the condition of finite concentration at $x^* \to \infty$ may be written as

$$c^* = \sum_{n=0}^{\infty} A_n f_n(z^*) \mathrm{e}^{-\beta_n^2 x^*} \tag{34}$$

in which A_n is the constant of integration and β_n designates the real eigenvalue associated with the eigenfunction f_n. By substituting Eq. 34 into Eqs. 31 and 32, it is straightforward to show that the function f_n satisfies the following differential equation

$$\frac{d^2 f_n}{dz^{*2}} + \beta_n^2 \left(\frac{D^* \beta_n^2}{Pe^2} + u_m^*\right) f_n = 0, \quad \left.\frac{\mathrm{d}f_n}{\mathrm{d}z^*}\right|_{z^*=\pm\alpha} = 0 \tag{35}$$

The solution of Eq. 35 provides the following formula

$$f_n = \cos\left[n\pi(z^*/\alpha + 1)/2\right] \tag{36}$$

$$\beta_n^2 = \frac{Pe\sqrt{Pe^2 u_m^{*2} + n^2\pi^2 D^*/\alpha^2} - u_m^* Pe^2}{2D^*} \tag{37}$$

wherein $n = 0, 1, 2, \cdots$. Applying the inlet boundary conditions to the concentration distribution (34), multiplying the resultant equation by f_m, integrating over z^* from $-\alpha$ to $+\alpha$, and finally following the application of the orthogonality condition, the constants A_n are obtained as

$$A_0 = \frac{1}{2}, \quad A_{2k+1} = \frac{2(-1)^{k+1}}{(2k+1)\pi}, \quad A_{2k+2} = 0 \text{ where } k = 0, 1, 2, \cdots \tag{38}$$

The final form of the concentration distribution will, therefore, become

$$c^* = \frac{1}{2} - \frac{2}{\pi}\sum_{k=0}^{\infty} \frac{(-1)^k}{2k+1} \cos\left[(2k+1)\pi(z^*/\alpha + 1)/2\right] \mathrm{e}^{-\beta_{2k+1}^2 x^*} \tag{39}$$

Mixing Index

Once the concentration field has been obtained, the parameters of physical interest can be calculated. Different parameters are used in the literature to quantify the degree of mixing in a T-sensor among which is the mixing index defined as

$$I_{\mathrm{mix}} = \frac{2c_m}{c_0} = 2c_m^* = \frac{2}{\alpha}\int_{-\alpha}^{0}\int_{0}^{1} c^* dy^* dz^* \tag{40}$$

As is clear from Eq. 40, c_m is the mean concentration over the half of channel cross section for which $z^* < 0$. A higher value of I_{mix} represents a more completed process of mixing. In fact, theoretically, I_{mix} reaches unity wherever mixing is completed. It is easy to verify that the mixing index is of the following simple form for our case

$$I_{\mathrm{mix}} = 1 - \frac{8}{\pi^2}\sum_{k=0}^{\infty} \frac{\mathrm{e}^{-\beta_{2k+1}^2 x^*}}{(2k+1)^2} \tag{41}$$

Table 1. Practical Ranges of Main Governing Parameters

Parameter	Value
Debye length λ_D[43,44]	1−500 nm
Diffusivity D[45]	43−100 μm^2 s^{-1}
Extensibility coefficient ϵ[46]	0−0.5
Fluid relaxation time Y[46,50]	0−25 s
Half channel height H[47]	5−100 μm
Half channel width W[48]	0.5−50 H
Helmholtz–Smoluchowski velocity u_{HS}[47]	10^{-7}−10^{-3} ms^{-1}

Results and discussion

It was found that four dimensionless factors including α, K, ϵWe^2, and Pe govern the transport of neutral species dissolved in viscoelastic fluids within an electrokinetically actuated T-sensor. In this section, a parametric study is executed to find out the degree to which each parameter affects the species transport phenomena. For ensuring the usefulness of the results, the dimensionless governing parameters are selected in accordance with the practical ranges of the physical parameters, provided in Table 1.

We start the discussion of results by an evaluation of the dimensionless effective diffusivity in Figure 2 that plots D^* vs. ϵWe^2 at different EDL thicknesses characterized by K. It is observed that the effective diffusivity grows by an increase in the level of elasticity in the fluid. This may be explained by considering the effects of ϵWe^2 on the velocity distribution. An increase in this parameter gives rise to the fluid behaving more like solids due to more effects of elasticity. Accordingly, the fluid particles tend to move under the same velocities, resulting in the increase of fluid velocity, especially near the wall.[49] So a nonuniform EOF of viscoelastic fluids causes more dispersion of solutes as compared to that of a Newtonian fluid. Figure 2 shows that this difference is quite significant and may lead to an order of magnitude difference in the pertinent values of D^* in some cases. Another point taken from this figure is that smaller EDLs are accompanied by lower values of the effective diffusivity. This is not surprising as more uniform velocity profiles are established for thinner EDLs.

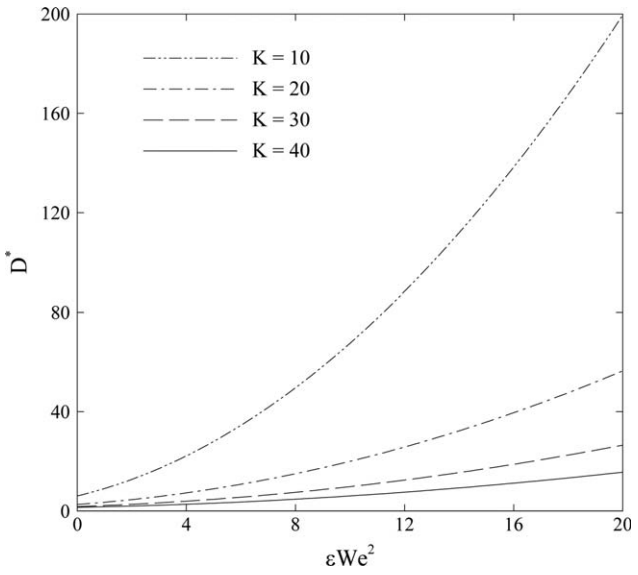

Figure 2. The dimensionless effective diffusivity as a function of εWe^2 at different EDL thicknesses, while keeping $Pe = 50$.

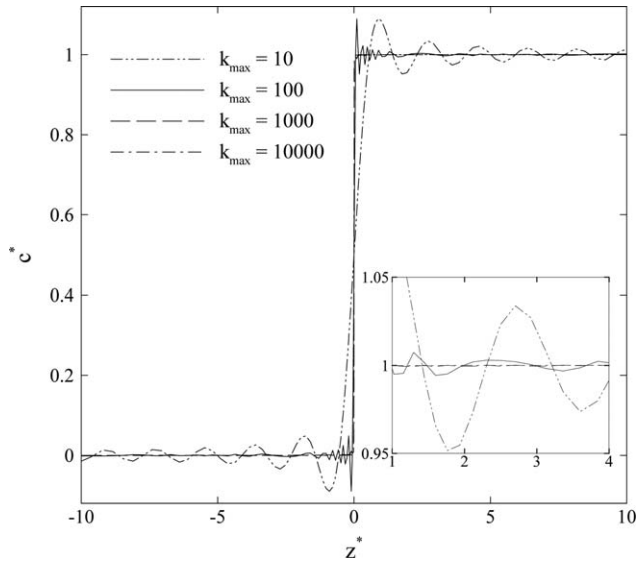

Figure 3. Convergence analysis for c^* at the inlet, considering $\alpha=10$; k_{max} is the number of series terms utilized in calculations.

Before proceeding further, it is crucial to make an estimate of the accuracy achieved by considering k_{max} terms of the series solutions. Since the accuracy decreases by approaching the merging junction, a convergence analysis should be done for the concentration distribution at the inlet. Figure 3 presents such an analysis by considering four different values of k_{max}. It is clear that, even in the inset, the concentration distributions obtained by utilizing 1000 and 10,000 terms of the series in Eq. 39 are indistinguishable. Hence, the latter is considered in all subsequent results.

A typical evolution of the concentration profiles along the axial direction is demonstrated in Figure 4. As seen, the inlet conditions are almost exactly satisfied by considering 10,000 terms of the series solution. All of the graphs pass through the point $c^*=0.5$ at centerline. This is the mean value that the thin layer of fluid at the interface between the two streams reaches almost immediately after the junction due to the infinite concentration gradient therein and retains it thereafter since there is no tendency to change. At $x^*=1$ one can observe a significant growth of the inter-diffusion zone as a result of considerable concentration gradients. The rate of the growth of the inter-diffusion area, however, decreases rapidly and, as observed, a dimensionless length of 300 is needed for the mixing to complete.

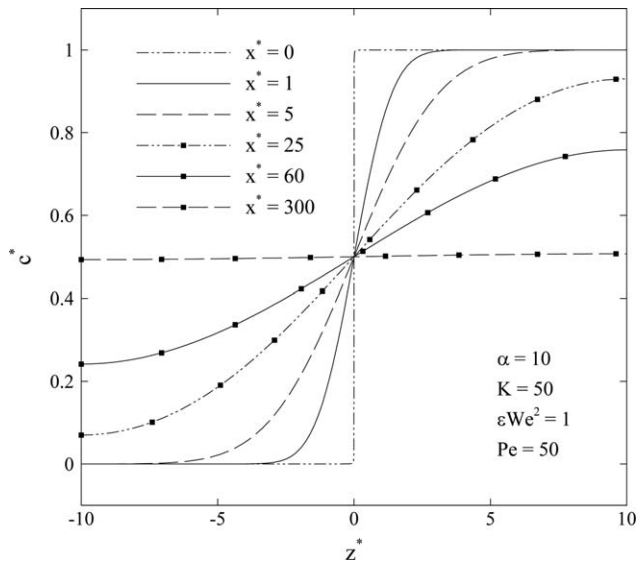

Figure 4. Evolution of the concentration profiles along the axial direction.

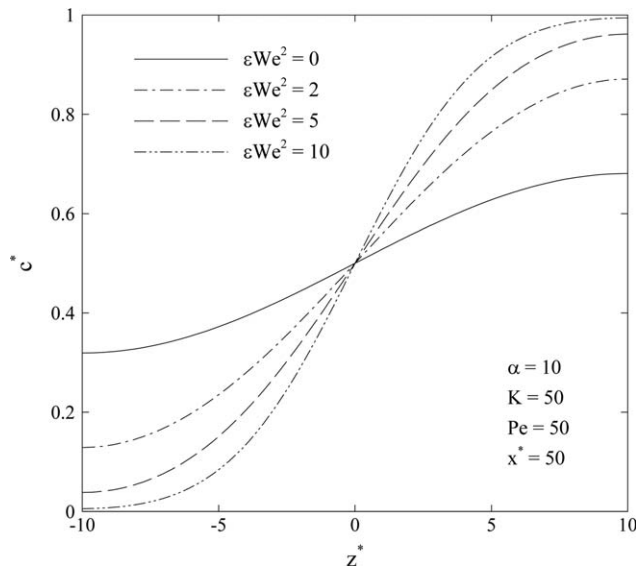

Figure 5. Profiles of c^* vs. z^* at different levels of elasticity in the fluid.

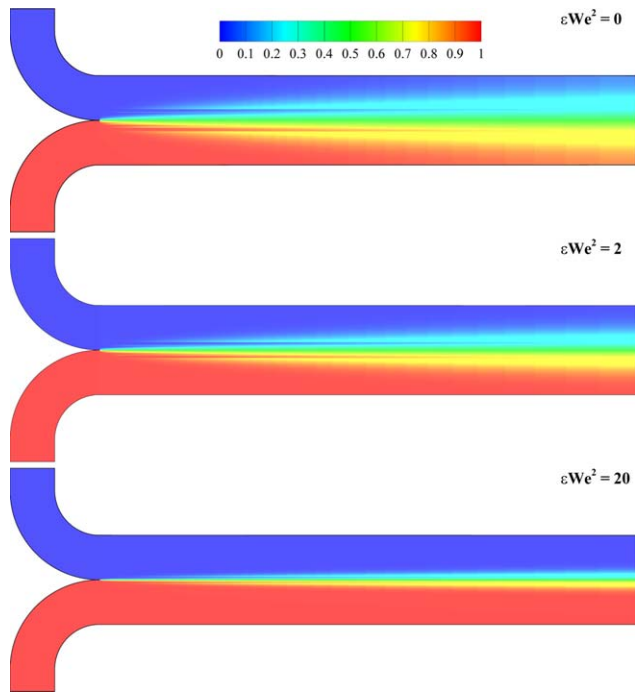

Figure 6. Concentration contours within the micromixer at different levels of elasticity considering $\alpha=8$, $K=50$, and $Pe=10$.

The dimensionless axial coordinate has been here multiplied by the Peclet number to get a better insight into the physics of the mixing process. [Color figure can be viewed in the online issue, which is available at wileyonlinelibrary.com.]

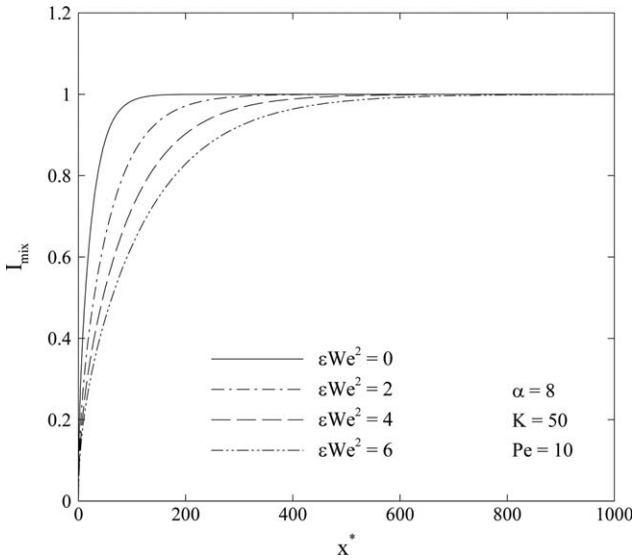

Figure 7. Variations of I_{mix} along the axial direction at different values of ϵWe^2.

Figure 5 depicts the dimensionless concentration profiles at different levels of elasticity in the fluid, while keeping x^* at 50. According to the previous discussions, decreasing ϵWe^2 will lead to a decrease in the electroosmotic velocity; this, in turn, gives rise to an increase in the solute residence time and cross-stream diffusion effects. The ultimate effect of decreasing ϵWe^2 is to get more uniform concentration profiles, as observed in Figure 5. The effects of the fluid rheology on the diffusion zone is more visible in Figure 6 which provides the concentration contours for three different values of ϵWe^2. According to the graphs, whereas the interdiffusion zone encompasses almost the whole channel cross section for the Newtonian fluid, the majority of the domain has not still felt the effects of diffusion when $\epsilon We^2=20$. Note that the dimensionless axial coordinate has been multiplied by Pe in this figure to get a better insight into the physics of the mixing process.

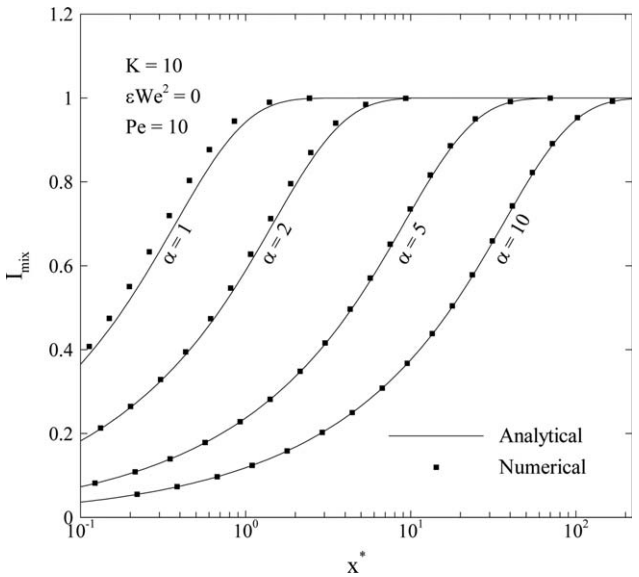

Figure 8. Plots of I_{mix} vs. x^* at different aspect ratios of the main channel.

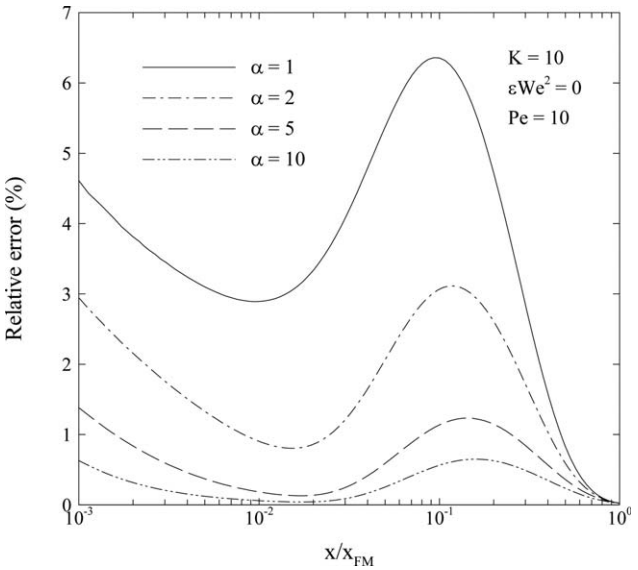

Figure 9. Relative error in calculating I_{mix} over the mixing length.

The axial coordinate is normalized by x_{FM} corresponding to the fully mixed situation where $I_{mix}=0.999$.

So far, we have only known that the mixing length is larger when elasticity effects show up. To obtain a quantitative estimate of the degree to which the level of elasticity in the fluid increases the mixing length, we make use of the mixing index. In Figure 7, the variations of this parameter in the axial direction is shown for four different values of ϵWe^2. A considerable increase of the mixing length is observed when elasticity effects are included. More precisely, the dimensionless mixing length, corresponding to $I_{mix}=0.999$, is increased from about 172 for a Newtonian fluid to 862 corresponding to $\epsilon We^2=6$. This is to say that approximately 400% increase in the mixing length occurs by introducing only a small amount of elasticity into the fluid rheological behavior. We call $\epsilon We^2=6$ small, since much higher values may be encountered in practice. For example, considering blood as the working fluid with a relaxation time of 0.001 s,[50] the Weissenberg number is computed to be 100, assuming $u_{HS}=1$ mms^{-1} and $\lambda_D=10$ nm.[43] This value is so high that even by considering ϵ to be of the order 0.01 the parameter ϵWe^2 will attain much higher values than those considered in Figure 7. This means that neglecting the nonlinear rheological behavior of biofluids may give rise to even an order of magnitude underestimation of the mixing length in some practical situations. This is in agreement with the experimental results reported by Bryce and Freeman[51] that indicated a strong reduction of mixing when adding minute amounts of polymers to liquids, causing viscoelasticity, in electroosmotic pumping.

Since our model neglects the sidewall effects on the velocity profile and Taylor dispersion coefficient, it should depend strongly on the channel aspect ratio. To determine the threshold value of α after which our model becomes reasonably accurate, the results are compared with the predictions of numerical simulations of the governing equations with which the assumptions of small zeta potential, 1-D velocity field, and negligible depthwise concentration variations are relaxed. The numerical method consisted of mapping the solution domain into the computational domain, according to the transformations given by Yavari et al.,[52] to cluster the grids in the regions

of high gradient. The transformed governing equations were then discretized utilizing a central finite-difference procedure of second order precision. Afterward, the resultant set of algebraic equations were solved by means of the Tri-Diagonal Matrix Algorithm (TDMA) with a relative convergence criterion of 10^{-9}. To ensure the grid independency of the results, an extensive analysis was performed, revealing that 100, 100, and 200 grids in x, y, and z directions, respectively, are sufficient to provide grid independent results. The comparison between the results of the two approaches, shown in Figure 8, reveals that the analytical model provides a reasonable estimation of the mixing efficiency even when $\alpha=1$. The associated relative errors shown in Figure 9 denote that the maximum discrepancy for this case is only about 6%. The developed model becomes more effective by increasing α and the analytical results are almost the same as the predictions of the numerical simulations when $\alpha=5$ for which the maximum relative error becomes only about 1%. It is worth noting that the errors in Figure 9 are reliable only after the first local minima because the numerical results themselves are not accurate before that due to the smallness of I_{mix} along with strong concentration gradients therein. So the actual errors should increase from zero to the maximums given in the figure. This is consistent with the physics of mass transfer since the species transport is mainly determined by diffusion at the early stages of development and the velocity distribution has a little effect and it can only take part when the concentration gradients in the transverse direction have been sufficiently diminished.

Apart from the estimation of error, Figure 8 may also be utilized to study the functionality of the mixing length on the channel aspect ratio. Before proceeding with the clarification of the aspect ratio effects on the mixing process, it is convenient to initially evaluate those of both dimensions H and W of the mixing channel. A larger channel height leads to a more rapid mixing of solutes, as the interface area between the two entering streams is increased. On the other hand, it is evident that the time needed for the solutes to fully spread out across the channel increases by decreasing the channel width. Hence, it can be deduced that a higher value of the ratio $H/W=\alpha^{-1}$ is corresponding to a faster mixing; that is mixing is improved by decreasing the channel aspect ratio, as justified by Figure 8.

Conclusions

Consideration was given to the cross-stream diffusion of an electrically neutral solute in an electrokinetic-based T-sensor. Of special interest was the influence of the fluid rheological behavior on the mixing process. As the flow of most biofluids of practical importance may be captured by viscoelastic constitutive equations, two of such models namely PTT and FENE-P were chosen to derive an approximate analytical solution for species transport. The solution presented assumes a negligible depthwise concentration gradient and adopts a 1-D velocity profile. It was observed that the maximum error introduced by these premises decreases to about 1% for an aspect ratio of 5 and may decrease more by considering larger aspect ratios. In addition, the examination of the rheology effects revealed a very strong dependency of the mixing length on the level of elasticity in the fluid, characterized by Weissenberg number. In this respect, it was observed that introducing even a small amount of elasticity into the fluid may result in an order of magnitude larger mixing lengths; accordingly, one may drastically underestimate the mixing length by considering the rheological behavior of biofluids to be linear. Last but not least, the Taylor dispersion coefficient for electroosmotic flow of viscoelastic fluids was obtained as a part of the analysis, founding it to be an increasing function of both the Weissenberg number and the Debye length.

Acknowledgment

The author sincerely thanks Iran's National Elites Foundation (INEF) for their supports during the course of this work.

Notation

A_n = constant of integration
c = number concentration, m^{-3}
c_{da} = depthwise averaged concentration, m^{-3}
c_m = mean concentration, m^{-3}
c_0 = inlet concentration, m^{-3}
D = diffusivity, m^2s^{-1}
D_{eff} = effective diffusivity, m^2s^{-1}
e = proton charge, C
$\mathbf{E}$ = electric field, Vm^{-1}
E_x = electric field in the axial direction, Vm^{-1}
f_n = eigenfunction
$\mathbf{F}$ = body force vector, Nm^{-3}
H = half channel height, m
I_{mix} = mixing index, $=2c_m/c_0$
k_B = Boltzmann constant, JK^{-1}
n_0 = ion concentration at neutral conditions, m^{-3}
$\mathbb{N}$ = number of ionic species in solution
Pe = Peclet number, $=u_{\text{HS}}H/D$
t = time, s
T = absolute temperature, K
u_{HS} = Helmholtz–Smoluchowski velocity, ms^{-1}
u_m = mean velocity, ms^{-1}
u_x = axial velocity, ms^{-1}
$\mathbf{u}$ = velocity vector, ms^{-1}
W = half channel width, m
We = Weissenberg number, $=\text{Y}u_{\text{HS}}/\lambda_D$
x, y, z = coordinates, m
$\tilde{x}$ = axial coordinate of moving reference frame, m
$\mathbb{z}$ = valence number of ions in solution

Greek letters

α = channel aspect ratio, $=W/H$
β_n = eigenvalue
$\dot{\boldsymbol{\gamma}}$ = strain rate tensor, s^{-1}
ε = fluid permittivity, $\text{CV}^{-1}\text{m}^{-1}$
ϵ = extensibility coefficient
ζ = zeta potential, V
K = dimensionless Debye–Hückel parameter, $=H/\lambda_D$
λ_D = Debye length, m
Λ = stress coefficient function
μ = viscosity coefficient, Pas
ρ = fluid density, kgm^{-3}
ρ_e = net electric charge density, Cm^{-3}
Y = fluid relaxation time, s
τ = stress tensor component, Pa
$\boldsymbol{\tau}$ = stress tensor, Pa
ψ = EDL potential, V

Superscripts

∇ = upper convected derivative
$*$ = dimensionless variable

Literature Cited

1. Reuss FF. Charge-induced flow. *Proc Imp Soc Nat Moscow*. 1809;3: 327–344.
2. Ghallab YH, Badawy W. *Lab-on-a-Chip; Techniques, Circuits, and Biomedical Applications*. Norwood, MA: Artech House, 2010.
3. Kamholz AE, Weigl BH, Finlayson BA, Yager P. Quantitative analysis of molecular interaction in a microfluidic channel: the T-sensor. *Anal Chem.* 1999;71:5340–5347.

4. Kamholz AE, Yager P. Theoretical analysis of molecular diffusion in pressure-driven laminar flow in microfluidic channels. *Biophys J*. 2001;80:155–160.
5. Kamholz AE, Yager P. Molecular diffusive scaling laws in pressure-driven microfluidic channels: deviation from onedimensional Einstein approximations. *Sens Actuators B Chem*. 2002;82:117–121.
6. Ismagilov RF, Stroock AD, Kenis PJA, Whitesides G, Stone HA. Experimental and theoretical scaling laws for transverse diffusive broadening in two-phase laminar flows in microchannels. *Appl Phys Lett*. 2000;76(17):2376–2378.
7. Beard DA. Taylor dispersion of a solute in a microfluidic channel. *J Appl Phys*. 2001;89(8):4667–4669.
8. Gobby D, Angeli P, Gavriilidis A. Mixing characteristics of T-type microfluidic mixers. *J Micromech Microeng*. 2001;11(2):126–132.
9. Wang H, Iovenitti P, Harvey E, Masood S. Optimizing layout of obstacles for enhanced mixing in microchannels. *Smart Mater. Struct*. 2002;11:662–667.
10. Holden MA, Kumar S, Castellana ET, Beskok A, Cremer PS. Generating fixed concentration arrays in a microfluidic device. *Sens Actuators B Chem*. 2003;92 199–207.
11. Wu Z, Nguyen NT, Huang X. Nonlinear diffusive mixing in microchannels: theory and experiments. *J Micromech Microeng*. 2004; 14(4):604–611.
12. Lam YC, Chen X, Yang C. Depthwise averaging approach to cross-stream mixing in a pressure-driven microchannel flow. *Microfluid Nanofluid*. 2005;1(3):218–226.
13. Sullivan SP, Akpa BS, Matthews SM, Fisher AC, Gladden LF, Johns ML. Simulation of miscible diffusive mixing in microchannels. *Sens Actuators B Chem*. 2007;123:1142–1152.
14. Bothe D, Lojewski A, Warnecke H-J. Fully resolved numerical simulation of reactive mixing in a T-shaped micromixer using parabolized species equations. *Chem Eng Sci*. 2011;66(24):6424–6440.
15. Ait Mouheb N, Montillet A, Solliec C, Havlica J, Legentilhomme P, Comiti J, Tihon J. Flow characterization in T-shaped and cross-shaped micromixers. *Microfluid Nanofluid*. 2011;10(6):1185–1197.
16. Broboana D, Balan CM, Wohland T, Balan C. Investigations of the unsteady diffusion process in microchannels. *Chem Eng Sci*. 2011; 66:1962–1972.
17. Chakraborty D, Bose N, Sasmal S, Dasgupta S, Maiti TK, Chakraborty S, DasGupta S. Effect of dispersion on the diffusion zone in two-phase laminar flows in microchannels. *Anal Chim Acta*. 2012;710:88–93.
18. Mouheb NA, Malsch D, Montillet A, Solliec C, Henkel T. Numerical and experimental investigations of mixing in T-shaped and cross-shaped micromixers. *Chem Eng Sci*. 2012;68:278–289.
19. Li Y-J, Li Y, Cao T, Qin K-R. Transport of dynamic biochemical signals in steady flow in a shallow Y-shaped microfluidic channel: effect of transverse diffusion and longitudinal dispersion. *J Biomech Eng*. 2013;135:121011.
20. Minakov A, Rudyak V, Dekterev A, Gavrilov A. Investigation of slip boundary conditions in the T-shaped microchannel. *Int J Heat Fluid Flow*. 2013;43:161–169.
21. Matsunaga T, Lee H-J, Nishino K. An approach for accurate simulation of liquid mixing in a T-shaped micromixer. *Lab Chip*. 2013;13: 1515–1521.
22. Erickson D, Li D. Influence of surface heterogeneity on electrokinetically driven microfluidic mixing. *Langmuir*. 2002;18(5): 1883–1892.
23. Wang Y, Lin Q, Mukherjee T. A model for laminar diffusion-based complex electrokinetic passive micromixers. *Lab Chip*. 2005;5: 877–887.
24. Jeong S, Park J, Kim JM, Park S. Microfluidic mixing using periodically induced secondary potential in electroosmotic flow. *J Electrostat*. 2011;69:429–434.
25. Ahmadian Yazdi A, Sadeghi A, Saidi MH. Rheology effects on cross-stream diffusion in a Y-shaped micromixer. *Colloids Surf A*. 2014;456(1):296–306.
26. Zhao C, Zholkovskij E, Masliyah J, Yang C. Analysis of electroosmotic flow of power-law fluids in a slit microchannel. *J Colloid Interface Sci*. 2008;326(2):503–510.
27. Zhao C, Yang C. Nonlinear Smoluchowski velocity for electroosmosis of Power-law fluids over a surface with arbitrary zeta potentials. *Electrophoresis*. 2010;31(5):973–979.
28. Vasu N, De S. Electroosmotic flow of power-law fluids at high zeta potentials. *Colloids Surf A*. 2010;368(1–3):44–52.
29. Babaie A, Sadeghi A, Saidi MH. Combined electroosmotically and pressure driven flow of power-law fluids in a slit microchannel. *J Nonnewtonian Fluid Mech*. 2011;166(14–15):792–798.
30. Vakili MA, Sadeghi A, Saidi MH, Mozafari AA. Electrokinetically driven fluidic transport of power-law fluids in rectangular microchannels. *Colloids Surf A*. 2012;414:440–456.
31. Das S, Chakraborty S. Analytical solutions for velocity, temperature and concentration distribution in electroosmotic microchannel flows of a non-Newtonian bio-fluid. *Anal Chim Acta*. 2006;559(1):15–24.
32. Mondal S, De S. Effects of non-Newtonian power law rheology on mass transport of a neutral solute for electro-osmotic flow in a porous microtube. *Biomicrofluidics*. 2013;7(4):044113.
33. Afonso AM, Alves MA, Pinho FT. Analytical solution of mixed electro-osmotic/pressure driven flows of viscoelastic fluids in microchannels. *J Nonnewtonian Fluid Mech*. 2009;159(1–3):50–63.
34. Masliyah JH, Bhattacharjee S. *Electrokinetic and Colloid Transport Phenomena*, 1st ed. New Jersey: Wiley, 2006.
35. Debye P, Hückel E. Zur Theorie der Elektrolyte. I. Gefrierpunktserniedrigung und verwandte Erscheinungen. *Physikalische Zeitschrift*. 1923; 24:185–206.
36. Sadeghi A, Yavari H, Saidi MH, Chakraborty S. Mixed electroosmotically and pressure-driven flow with temperature-dependent properties. *J Thermophys Heat Transfer*. 2011;25(3):432–442.
37. Thien NP, Tanner RI. A new constitutive equation derived from network theory. *J Nonnewtonian Fluid Mech*. 1977;2(4):353–365.
38. Phan-Thien N. A nonlinear network viscoelastic model. *J Rheol (1978-present)*. 1978;22(3):259–283.
39. Taylor G. Dispersion of soluble matter in solvent flowing slowly through a tube. *Proc R Soc London Ser A*. 1953;219(1137):186–203.
40. Probstein RF. *Physicochemical Hydrodynamics*, 2nd ed. New York: Wiley, 1994.
41. Aris R. On the dispersion of a solute in a fluid flowing through a tube. *Proc R Soc London Ser A*. 1956;235:67–77.
42. Bird RB, Stewart WE, Lightfoot EN. *Transport phenomena*, 2nd ed. New York: Wiley, 2002.
43. Karniadakis G, Beskok A, Aluru N. *Microflows and Nanoflows, Fundamentals and Simulation*. New York: Springer, 2005.
44. Maynes D, Webb BW. The effect of viscous dissipation in thermally fully-developed electro-osmotic heat transfer in microchannels. *Int J Heat Mass Transfer*. 2004;47(5):987–999.
45. Gervais T, Jensen KF. Mass transport and surface reactions in microfluidic systems. *Chem Eng Sci*. 2006;61(4):1102–1121.
46. Campo-Deano L, Dullens RPA, Aarts DGAL, Pinho FT, Oliveira MSN. Viscoelasticity of blood and viscoelastic blood analogues for use in polydymethylsiloxane in vitro models of the circulatory system. *Biomicrofluidics*. 2013;7:034102.
47. Kandlikar SG, Garimella S, Li D, Colin S, King MR. *Heat Transfer and Fluid Flow in Minichannels and Microchannels*. Oxford: Elsevier, 2006.
48. Nguyen N-T, Wu Z. Micromixers-a review. *J Micromech Microeng*. 2005;15:R1–R16.
49. Sadeghi A, Veisi H, Saidi MH, Asghar Mozafari A. Electroosmotic flow of viscoelastic fluids through a slit microchannel with a step change in wall temperature. *J Heat Transfer*. 2013;135(2):021706.
50. Thurston GB. Rheological parameters for the viscosity, viscoelasticity and thixotropy of blood. *Biorheology*. 1979;16:149–162.
51. Bryce RM, Freeman MR. Abatement of mixing in shear-free elongationally unstable viscoelastic microflows. *Lab Chip*. 2010;10:1436–1441.
52. Yavari H, Sadeghi A, Saidi MH, Chakraborty S. Temperature rise in electroosmotic flow of typical non-newtonian biofluids through rectangular microchannels. *J Heat Transfer*. 2014;136(3):031702.

Manuscript received Mar. 12, 2015, and revision received June 23, 2015.